A Study of Flare Emission in DV Psc using TESS

Deblina Lahiri (lahiri.deblina1997@gmail.com)
Osmania University
Mamatha Rani Gaddam
Osmania University
Sriram Kandulapati
Osmania University

Research Article

Keywords: binaries, eclipsing—stars, activity—stars, flare—stars, late-type starspots, individual, DV Psc

Posted Date: July 20th, 2023

DOI: https://doi.org/10.21203/rs.3.rs-3176188/v1

Additional Declarations: No competing interests reported.

A Study of Flare Emission in DV Psc using TESS

Deblina Lahiri, [1] • G. Mamatha Rani, [1] • K. Sriram [1]

Abstract We report the detection of two superflares along with other eight relatively moderate flares in a close binary RS CVn system DV Psc using TESS data. The flare energies were found to be in the range 0.24–23.97 $\times$ 10^{34} erg with a duration of a few minutes to close to an hour. Most of the flares were not observed in the primary and secondary minima phases. The two superflares occurred at a phase of 0.1 and 0.55 and the stellar spot with a magnetic field B=500-2000 G can explain the energetics. Since the period of the binary is increasing, we estimated the energy due to mass transfer and noted that accretion energy may provide energy for the flares. Based on the sample of flaring late-type star data, we noted that flares in DV Psc possibly may arrive from either of the stellar components as the correlation between Log E vs Log R does agree well with theoretical relation (E$\propto$ R^3). Based on the values of the rotation period for both stellar components, we conclude that DV PSc displays low flaring frequency for a fast rotator. The loop lengths were estimated at 3.65–4.55 $\times$ 10^{10} cm for superflare events which were $\sim$ three times less than the separation (1.40 $\times$ 10^{11} cm) but if both loops occur at a similar time, the loops may interact and can trigger the observed superflares. We conclude that a large stellar spot or interconnecting magnetic field of lines among binary companions may trigger the superflares.

Keywords binaries: eclipsing—stars: activity—stars: flare—stars: late-type starspots:— individual:— DV Psc

Deblina Lahiri,

G. Mamatha Rani,

K. Sriram

Department of Astronomy, Osmania University, Hyderabad, 500007, India

1 Introduction

The study of eclipsing binary (EB) systems are important as they furnish information regarding stellar evolution and their interior structures, via their mutual interactions, magnetic activity, and variations. Among these are the class of active binaries known as the RS Canum Venaticorum systems (RS CVns) binaries. In these systems, the two stellar companions are tidally locked although they do not undergo any mass transfer making them a detached system. In general, one of the stars has the spectral type F to G dwarf or a subgiant which is $\sim$1000 K hotter than its companion. These systems are divided into three subgroups based on their orbital period as, the short period (P$\leq$1d), classical (1d$\leq$ P $\leq$14d), and long period (P$\geq$14d). The X-ray luminosity of such sources is L_X = 10^{29}–10^{32} erg s^{-1} (Drake et al. 1989; Dempsey et al. 1993), and produces stellar flares and spots. The stars in RS CVn systems are late-type in nature and hence are fully convective or the upper portion of its interior has a convective layer that leads to the presence of magnetic dynamo. Thus it can be a strong reason for the appearance of spots on either or both the stellar components and also the magnetic reconnection that leads to energy release in stellar flares (Hilton et al. 2011; Lin et al. 2019).

Stellar flares are rapid events that are highly energetic in nature that takes place during magnetic reconnection in the coronae of the stars Kowalski et al. 2010; Shibayama et al.2013). It is produced when non-potential magnetic energy is converted into other forms of energy during a very short period of time. These flares are also thought to be associated with the release of magnetic energy stored in the star spot (e.g. Shibata & Magara 2011). The acceleration electrons along the magnetic field lines traversing towards the photosphere cause the heating of the plasma to drastically increase the temperature above 20 MK. The wavelength

of radiating energy is determined by the depth at which the electrons decelerate during the flare. The increasing flaring activity depends on the magnetic field and is found to depend on the rapid stellar rotation (eg. Wright et al. 2018), cool stars or late spectral type (Davenport et al. 2019), and large stellar spots (Yang et al. 2017). The time span of flaring events varies from minutes to hours, displaying a fast rise and an exponential decay (FRED) profile. Flare energies are in general found to be from 10^{26} to 10^{32} erg and the super-flare energies are $\geq 10^{34}$ (eg. Shibayama et al. 2013).

The superflare energy is related to large stellar spots and can be associated with the relation between solar flares-sunspots. The solar dynamo mechanism most probably causes the formation of large stellar spots and harbors the energy of superflares (Shibata et al. 2013). It is not always the case the spot shall produce the flares. Based on the Kepler database, It was noted that only 7% stars exhibited flares but found no correlation with the stellar spot phase or flare energy (Hawley et al. 2014; Doyle et al. 2018). There are other possible mechanisms for superflares like a hot Jupiter companion can cause superflares on a solartype star (Rubenstein & Schaefer 2000) also supported by the numerical simulation of planet-star magnetic interaction on the stellar activity (Ip et al. 2004). Instead of stellar spots, the superflares may be caused by faculae dominating the rotational modulation (He et al. 2018). It is also possible that the superflares are initiated due to the disruption of the interconnecting field lines for the RS CVn binary (Simon et al. 1980).

Flare events are also detected in close binaries. The strong mutual interaction between the components can induce magnetic activity (Noyes et al. 1984). Gao et al. (2016) have detected 236 flares in binaries using Kepler eclipsing binary database. RS Cvn variables also emit flare (eg. Pandey & Singh 2012). Sriram et al. (2023) detected flares including superflares in an RS CVn binary CF Tuc using TESS data and concluded that strong flares are closely associated with large spots whereas moderate amplitude flares have different origins. Qian et al. (2014) observed many flares in a contact binary with K spectral type CSTAR 038663 probably associated with the dark spot. Balona (2015) also detected flares in three eclipsing binaries and found no correlation between flares and the orbital phase. Flare events have been detected in a few other close binaries CU Cnc (Qian et al. 2012), GSC02314-00530 (Dimitrov & Kjurkchieva 2010), GJ3236 (Smelcer et al. 2017) and EVLac (Honda et al. 2018).

The first light curves of DV Psc were observed by Robb et al. (1999) reporting the presence of at least one spot on either of the components. It was Stephenson (1986) who for the first time classified the source as a K4-5 spectral type. Ever since this source was under study and its properties such as the asymmetry in light curve (Robb et al. 1999; Vaňko et al. 2007; Parimucha et al. 2010), the chromospheric activity evident from the Ca II H and K emissions (Beers et al.1994; Pi et al. 2014) and also its strong X-ray emission ((Bade et al.1998). Salchi & Edalati (2003) were able to explain the asymmetric nature of the light curve to be due to the presence of spots. The mass ratio of 0.702±0.014 from the radial velocity curve was reported by Lu et al. (2001). The orbital parameters of DV Psc were revised by Zhang & Zhang (2007) with BVR filters using a CCD camera along with the reported radial velocity curve. The source has shown significant spot variation as reported by Parimucha et al. (2010). The magnetic activity cycle for DV Psc was obtained by Pi et al. (2014) with a period of about 4.88±0.32 yr from the phase values 0.25 and 0.75 for Max I & Max II phase respectively. The flare occurrence probability was reported to be 0.082 flares per hour and also reported an upward parabola (period increasing) in the O-C orbital period diagram, which was interpreted to be arising due to mass transfer or magnetic braking.

Pi et al.(2019) have confirmed the presence of optical flares for the source along with period variation and star spot activity. Depending on the spot parameter gathered in previous years they have found a spot oscillation cycle with a period of about 3.60±0.03 yr and 3.42±0.02 yr for the 90° and 270° belts. As the period of the magnetic cycle in the O-C diagram is 13.26 yr which is much greater than the period found from the spot cycle therefore, the cyclic oscillation found in the O-C diagram is attributed to the presence of a third body rather than any active magnetic cycle. They detected a total of 21 flares in an observation of 326.4 hr and the flare frequency was 0.064 flares per hour. The flare energies obtained were determined to be 6.62×10^{31} erg to 1.10×10^{34} erg. For the source DV Psc, it was found that the phase of flares is closely associated with the spot location.

The source DV Psc is an RS CVn type binary system with the mass $0.68 \pm 0.02\ M_{\odot}$ & $0.47 \pm 0.02\ M_{\odot}$ for the primary and secondary components respectively. The temperature of the primary is about 4450 K and that of the secondary is 3680 K (see Gazeas & Palafouta 2019). Understanding the flares especially the superflares in RS CVn and constraining the underlying mechanism is important, hence we carried out a study on DV Psc based on the TESS data.

2 Observation

The observational data for the source DV Psc is from a space-based telescope the Transiting Exoplanet Sur-

vey Satellite (TESS). Launched in April 2018, TESS is positioned in a highly elliptical orbit, that has a period of 13.7 days that stabilizes the orbit in a 2:1 resonance with the Moon (Ricker et al. 2015). Its aim is to employ the transit method to look for exoplanets. It observes selected sectors of the sky using the four 10.5 cm telescopes onboard in the wavelength range 600-1000 nm for slightly less than a month's time. It has a field of view (FoV) 24° × 96°. The light curve obtained for the source DV Psc by TESS has a 2 minutes cadence provided publicly, that allows us to study a vast number of stellar flares with a high signal-to-noise ratio (SNR). For DV Psc the observation started on 2021-08-21, 04:31:38.12, and ended on 2021-10-11, 09:26:57.26. The short cadence Pre-searched Data Conditioning Simple Aperture Photometry (PDCSAP) light curves obtained from the Mikulski Archive for Space Telescopes (MAST)[1] are being used for carrying out the study on the detection of the stellar flares.

3 Flare detection method

The TESS observations for this particular source were slightly more than a month. As the purpose of this study is to detect stellar flares emitted by DV Psc, hence we have used the flare detection method elaborated in Sriram et al. (2023) based on the technique adopted by Shibayama et al. (2013). For the proper execution of the task and to avoid false detection of flare we have first removed the flux variation due to the binary nature of the source (eg. Sriram et al. 2023) as it is a binary system with a probable existence of a third body. A section of the light curve showing the two superflares (f1 & f3) along with a moderate flare (f2) is shown in Figure 1 (top panel). We have calculated the flux variation distribution (Figure 1, middle panel histogram) between all the successive data points in the light curve. The thick line in Figure 1 (histogram) shows the top 1% of the distribution and the dot-dashed line shows the three times of this top 1% which is regarded as the threshold of the flare. To avoid any further misdetections of other flux variations, the selection of our threshold was a result of a test run. The start time of the flares is determined whenever the flux was observed to be greater than the threshold value. The standard deviation of the distribution is obtained to determine the end time for the flares. These values of start (st) and end (et) times for all the flares are noted in Table 1. Figure 1 (bottom left panel) presents the spline fit of the largest flare obtained for this source, where the average of five points before the flare is denoted by a black point and the other two black points are the average of points after the flare. We have detected a total of 10 flares (f1–f10) using this method which is further confirmed by visual inspection and two of which can be considered as superflares discussed later in the paper.

Most of the flares that we have obtained here are classical in nature (i.e. FRED type), but we have also encountered some of the complex flares (f1, f3 & f5) that have double peaks feature and some of which have peaks almost of the same amplitude, similar to the ones observed in KIC 9048551 (eg. Kuznetsov & Kolotkov 2021).

4 Flare profile fitting

For the estimation of the flare parameters such as the starting time (st_f), peak time (pt_f), and decay time (τ_{decay}) that are important for calculating luminosity, energy, and the flare loop length. We have used the burst model for fitting the observed flares. The model used for this fitting consists of a fast rise ($F_{\rm rise}$) and an exponential decay ($F_{\rm decay}$) (FRED) profile where A is the normalization and also a constant where the brightness component is non-varying in the obtained normalized light curve, the function is defined as

$$\begin{aligned} F_{\rm rise} &= A\left[\frac{t-st}{pt-st}\right] \forall, st < t < pt; \\ F_{\rm decay} &= A \times exp\left[\frac{-(t-pt)}{\tau_{decay}}\right] \forall, pt < t \end{aligned} \quad (1)$$

All the parameters yielded from the above fitting along with the reduced χ^2 along with their uncertainties at 90% confidence level are provided in Table 1. Mostly, we have used a single burst profile to fit seven (f2, f4, f6, f7, f8, f9 & f10) of the flares and the remaining three (f1, f3 & f5) flares required a double burst profile in order to obtain a better fit (see, Figure 2, 3 & 4).

5 Energy Estimation of flares

We have calculated the energy of flares using two different methods as explained below:

5.1 Method 1: Based on flare luminosity

The estimation of the total energy of each flare from stellar luminosity, amplitude, and the flare duration as obtained from the flared profile assuming that the spectrum of flares can be expressed by blackbody radiation

[1] https://mast.stsci.edu.

having an effective temperature of 10,000 K denoted as $T_{\rm flare}$ based on the previous studies (Hawley and Pettersen 1991; Kowalski et al. 2013; Howard et al. 2018). The bolometric flare luminosity $L_{\rm flare}$ is calculated from $T_{\rm flare}$ and the area of flare $A_{\rm flare}$ using the equation below:

$$L_{\rm flare} = \sigma T_{\rm flare}^4 A_{\rm flare} \tag{2}$$

where σ is the Stefan–Boltzmann constant. As the star is not a blackbody radiator, the obtained values suffer inaccuracy with an error of some tens of percent. The flare area $A_{\rm flare}$ is calculated using, the following equation :

$$A_{\rm flare} = (\Delta F/F_{\rm av})\pi R_{\rm star}^2 \frac{\int R_\lambda B_\lambda(T_{\rm eff})d\lambda}{\int R_\lambda B_\lambda(T_{\rm flare})d\lambda} \tag{3}$$

where R_λ is the TESS response function, obtained from the product of the filter transmission and the detector quantum efficiency. Here, λ is the wavelength, $B_\lambda(T_{\rm eff})$ and $B_\lambda(T_{\rm flare})$ are the Planck functions evaluated for the star's effective temperature and the flare temperature. $R_{\rm star}$ is the radius of the stellar companion thought to be involved in the flare production, here we have calculated these values for both the stars (see Table 2 & 3) as both of them are magnetically active.

($\Delta\ F/F_{\rm av}$) the flare amplitude obtained from the flare profile (Shibayama et al. 2013; Notsu et al. 2019) shown in Table 1. $\Delta\ F = F$ - $F_{\rm av}$ where F is the stellar brightness and $F_{\rm av}$ is the average flux. The luminosities of the star and the flare in the observing bandpass of the instrument ($L_{\rm star}$ and $L_{\rm flare}$ respectively) can be obtained using the following equations

$$L_{\rm star} = \pi R_{\rm star}^2 \int R_\lambda B_\lambda(T_{\rm eff})d\lambda \tag{4}$$

$$L_{\rm flare} = A_{\rm flare}(t) \int R_\lambda B_\lambda(T_{\rm flare})d\lambda \tag{5}$$

As $L_{\rm flare}$ is a function of time. The total bolometric energy of the flare $E_{\rm flare}$ is basically as integral of the luminosity of flare $L_{\rm flare}$ throughout the flare duration and can be estimated from the following equation

$$E_{\rm flare} = \int L_{\rm flare}(t)dt \tag{6}$$

The flare luminosity, flare area, and the respective energy of the observed flares are shown in Table 2 & 3 for the primary and secondary components of the source respectively.

5.2 Method 2: Based on spot area

We have determined the area of stellar spot ($A_{\rm spot}$) using the equation (Maehara et al. 2012; Shibata et al. 2013)

$$A_{\rm spot} = \frac{\Delta F_{\rm spot}}{F}(A_{\rm star})\left[1 - \left(\frac{T_{\rm spot}}{T_{\rm star}}\right)^4\right]^{-1} \tag{7}$$

where $\frac{\Delta F_{\rm spot}}{F}$ is the amplitude of the flux variation caused by due to the spot that is normalized by the average flux. $A_{\rm star}$ is the area of the star and $T_{\rm star}$ and $T_{\rm spot}$ are temperatures of the star photosphere and the star spot respectively.

The temperature difference between the star photosphere and the star spot $T_{\rm star}$-$T_{\rm spot}$ is deduced from the following equation (Maehara et al. 2017; Berdyugina 2005):

$$\begin{aligned}\Delta T(T_{\rm star}) &= T_{\rm star} - T_{\rm spot} \\ &= 3.58\times10^{-5}T_{\rm star}^2 + 0.249\,T_{\rm star} - 808\end{aligned} \tag{8}$$

where $T_{\rm star}$ is the temperature of the un-spotted photosphere of the primary and secondary components i.e. 4450 K and 3692 K respectively (Gazeas & Palafoua 2019) and $T_{\rm spot}$ is the spot temperature of the respective components.

A revised version of the above equation was proposed by Herbst et al. (2021) based on more data on stellar flares

$$\begin{aligned}\Delta T(T_{\rm star}) &= T_{\rm star} - T_{\rm spot} \\ &= 3.58\times10^{-5}T_{\rm star}^2 + 0.0188\,T_{\rm star} - 239.3\end{aligned} \tag{9}$$

For calculating the upper limit of flare energy $E_{\rm Sflare}$ we have used a simple scaling law as described in Shibata et al. (2013). The occurrence flares are thought to be the abrupt release of the magnetic energy that is stored in the star spots. Hence, the total energy thus obtained should be less than or equal to the magnetic energy stored around these star spots. The $E_{\rm Sflare}$ is calculated from the area of the spot and the magnetic field strength as follows:

$$E_{\rm Sflare} = f \times E_{\rm mag} \sim f \times \frac{B^2(A_{\rm spot})^{3/2}}{8\pi} \tag{10}$$

where f is the fraction of magnetic energy (around 10%, Shibata et al. 2013) that can be released as the

energy of the flare, B is the magnetic field strength and $A_{\rm spot}$ is the area of the star spot obtained earlier from equation 7.

6 Results and Discussion

Based on TESS observations of an RS CVn DV Psc, we studied ten flares among which three have double peak profiles. Based on the estimation of the energy of the flares, it ranges from 0.24 –23.97 $\times$ 10^{34} erg with a duration of 778 s – 3542 s. We noted that most of the flare occurred at the phase where both stellar components are seen. Only on one occasion, the flare appears at phase ϕ=0.98, where the secondary component is along the line of the sight of the observer. The mutual tidal effects pivotally contribute to the enhancement of magnetic activity in the RS CVns (Cuntzetal. 2000). The density of magnetic field flux and its development around the binary could affect the flare distribution in the orbital phase (Holzwarth & Schüssler 2003a, 2003b). In a binary system, most of the flares should be seen during the largest cross-section along the line of sight at the orbital phases 0.25 and 0.75. Pi et al. (2014) observed that most of the flares in DV Psc are not occurring at primary and secondary minima. Similarly, Pi et al. (2019) observed fifteen flares mostly occurring at phase, ϕ = 0.3 - 0.4. Luo et al. (2019) observed that most of the flares occurred at ϕ = 0.6, where the space between the component where mass accretion is happening can be seen. They concluded that mass accretion from primary to secondary is most probably skewing the occurrence of flare at ϕ = 0.6. Balona (2015) found no significant dependency of flare frequency with the orbital phase in three eclipsing binaries with varying orbital periods. Gao et al. (2016) noted no correlation between flare frequency and orbital phase in two eclipsing binaries and a similar study for twenty non-eclipsing binaries displayed bimodal distribution of flares around phases 0.25 and 0.75. They concluded that this could be due to gravitational distortion and/or orbital inclination. Based on TESS observation of flares emitted by the source CF Tuc, Sriram et al. (2023) observed that flares mostly take place not in the primary and secondary minima, and hence there is no dependency on the orbital phase and flare frequency.

6.1 Are super flares associated with the mass transfer

The period variation of DV Psc is well studied (Pi et al. 2014) and it was noted that the orbital period is increasing with a mass accretion rate $\dot{m} = 0.37 \times 10^{-7}$ $M_\odot$ yr^{-1}. It is quite possible that this accretion can provide some energy to the flare. The luminosity due to the accretion can be estimated from the following equation

$$L_{\rm acc} = GM_1\dot{m}(\Omega_1 - \Omega_c)/D \quad (11)$$

where M_1 is primary star mass, Ω_1 and Ω are the potential of the stellar component and critical potential respectively and D is the distance between the two components. Gazeas & Palafouta (2010) reported Ω_1 = 3.533, Ω_c = 3.226 (for q=0.69 and synchronized system) and D is 1.40 $\times$ 10^{11} cm. The L_{acc} was estimated to be 1.54 $\times$ 10^{31} erg s^{-1} and for the largest flare F1, the duration of the flare is 3542 s which amounts to an energy E_{acc} = 1.72 $\times$ 10^{36} erg. This energy is eight times greater than the flare's energy E_f = 2.2 $\times$ 10^{35} erg. It is quite possible that some amount of accretion energy may contribute to the flare energy and the super flare could be caused due to this mass accretion. However, we could not observe significant distortion in any of the flare profiles when compared to flares emitted by single M-type stars.

6.2 Flares due to stellar spots

DV Psc stellar components are K and M-spectral types but the exact magnetic field strength is not known. However, based on the Zeeman Doppler Imaging (ZDI) method for RS CVn sources viz. II Peg (Kochukhov et al. 2013) and HR 1099 (Donati 1999; Petit et al. 2004), a complex magnetic field was observed with the strength of 500-1000 G. A threshold magnetic field strength of B = 500 G was noted by Howard et al. (2020) for K5-M4 spectral types. Shulyak et al. (2019) detect strong kG magnetic fields for 29 active M-type dwarfs for a short rotation period (P< 4d). For GT Peg with T = 3500 K and OT Ser T = 3600 K, the magnetic field strengths were determined to be $\sim$ 3000 G, where the temperatures are similar to the secondary M-type component of DV Psc. Torres et al. (2022) studied a K-spectral type eclipsing binary and estimated the magnetic field strength of about $\sim$ 1600-1800 G. We estimate the flare energy due to stellar spot using B=500 and 2000 G. For the first flare (f1) and third flare (f3) in the light curve, $\frac{\Delta F_{\rm spot}}{F}$ was found to be 0.066 and 0.031 respectively. Using equation 8, for f1 , the upper limit of flare energy $E_{\rm Sflare}$ = 0.22 $\times$ 10^{35} erg (B=500 G) and $E_{\rm Sflare}$ = 3.58 $\times$ 10^{35} erg (B = 2000 G) assuming the primary component. Using equation 9, for the same B values, $E_{\rm Sflare}$ = 0.43 $\times$ 10^{35} erg (B=500 G) and $E_{\rm Sflare}$ = 6.97 $\times$ 10^{35} erg (B=2000 G). Using the same magnetic field, for the third flare (f3), $E_{\rm Sflare}$ = 0.07 $\times$ 10^{35} erg (B=500 G) and $E_{\rm Sflare}$ = 1.14 $\times$ 10^{35} erg (B=2000 G) using equation 8 and $E_{\rm Sflare}$ = 0.14

$\times$ 10^{35} erg (B=500 G) and $E_{\rm Sflare}$ = 1.39 $\times$ 10^{35} erg (B=2000 G) using equation 9. As discussed above the magnetic field can be of the order of 3000 G for M-type, and hence the flare energy will be even more. The flares f1 and f3 can be classified as superflares ($\geq$ 10^{34} erg) and for B=500 G the flare energies due to spot ($E_{\rm Sflare}$) were smaller in magnitude compared to the calculated flare energy ($E_{\rm f}$) based on the flare profiles observed in the light curve. We suggest the magnetic field strength should be higher which is often seen from other studies.

6.3 Possible association of flares with stellar components

As most of the flare energies are around $\sim$ 10^{34} erg and two of them are found to be of the order of $\sim$ 10^{35} erg and these flares are found around phases $\sim$ 0.10 and $\sim$ 0.55 (see Table 1). At these phases, it is difficult to know from which stellar component these are arising. Gunther et al. (2020) studied flares emitting from M-type stars ranging from a temperature of 3000 - 6000 K using TESS data. We collected that and divided it into two bins of temperature (see Figure 5). The top panel displays the histogram of the flares energy distribution emitting from M-type stars with temperature 3000 - 4000 K (green marker) and the red one corresponds to the flares energy with temperature 3350 - 3850 K. Both distributions are fitted with Gaussian functions shown with thick lines with a mean μ, Log E= 33.03$\pm$0.004 erg and σ= 0.46$\pm$0.004 (green) and a mean μ, Log E= 33.32$\pm$0.01 erg and σ = 0.32$\pm$0.10 (red). A similar fitting procedure was adopted for the temperature bin of 4000 - 5000 K (green) and 4250 - 4650 K (red) (Figure 5, bottom panel). The fitting resulted in a mean μ, Log E = 33.97$\pm$0.01 erg and σ= 0.46$\pm$0.008 (green) and a mean μ, Log E= 34.13$\pm$0.20 erg and σ= 0.51$\pm$0.29 (red). The uncertainties quoted are 90% confidence level, $\Delta\chi^2$ =2.71. As the mean flare energies are matching the observed flare energy in DV Psc, we suggest that the observed flares are emitting from the primary component of the DV Psc.

The energy released in the stellar flares is due to the reconnection of the magnetic field lines which in turn depends on magnetic field strength B and the loop length L. The energy deposited in the loop is given by $E = L^3B^2/2\pi$ and in general the magnitude of B increase with the decrease in the temperature of the star associated with deep convection zones. Balona (2015) has shown that there exists a strong correlation between E and the radius of the star (R) assuming that L $\propto$ R^3. We also studied such a correlation for M-type star flares (Gunther et al. 2020) along with detected flares in DV Psc. A linear regression fit was performed which resulted in line Log E = 2.83(0.30) Log R/$R_\odot$ + 34.23(0.11) assuming that flares were arisen from primary and Log E = 2.68(0.35) Log R/$R_\odot$ + 34.36(0.14) for secondary component (see Figure 6). This clearly shows a departure from the theoretical relation E $\propto$ R^3 if the flares are arising from the secondary stellar component.

DV Psc is a short-period binary system and both stellar components are synchronized i.e. orbital period is equal to the rotation period. It is expected that rapidly rotating low-mass stars are anticipated to produce an increased level of activity which is associated with their respective dynamo mechanism (Maggio et al. 1987). It is also noted that with an increase in the rotation period, the activity level decreases (Kiraga & Stepien 2007; Yang et al. 2017). Doyle et al. (2019) noted that for nine fast rotators (< 0.3 d) with M-type spectral type, the flare occurrence was low when compared to the rotators with period P > 0.3 d. We also computed the rotation period for the primary and secondary components using the relation $\Omega = 2\pi R/P_{rot}$ where primary radius is R1 = 0.71 $R_\odot$ and secondary is R2 = 0.52 $R_\odot$. We found Ω_1 = 117.19 km s^{-1} and Ω_2= 85.82 km s^{-1}. We noted a flare frequency of 0.30 flare d^{-1}. These values show that DV Psc also displays low flaring frequency rate behavior similar to the fast single rotators (see Fig. 9 of Doyle et al. 2019). The exact reason for such a low flaring rate is not known but Doyle et al. (2022) suggest that the magnetic field configuration or the saturation effect is the possible reason.

In RS CVn the interacting magnetic field lines could trigger the flares (Simon et al. 1980), hence loop lengths were estimated. The flare loop length (L) was calculated by taking the flare decay time (τ_{decay}) and the flare energy ($E_{\rm flare}$) into account for the two superflares present in our study using the formula (Namekata et al. 2022)

$$L \sim 1.64 \times 10^9 \left[\frac{\tau_{decay}}{100(s)}\right]^{2/5} \left[\frac{E_{\rm flare}}{10^{30}(erg)}\right]^{1/5} cm \qquad (12)$$

The loop length for f1 over the primary was estimated to be L= 4.55$\times$ 10^{10} cm and for secondary L = 4.06 $\times$ 10^{10} cm. Similarly, loop length for f3 with primary L = 4.10$\times$ 10^{10} cm and with secondary L = 3.65 $\times$ 10^{10} cm. The loop lengths were smaller than the separation of the binary by a factor of 3. But if the loops are occurring at the same time on both the components then it is possible that they may interact and would initiate the superflares.

7 Conclusions

Based on TESS observations of DV Psc, two superflares and eight moderate amplitude flares were detected. The two superflares energies were close to $\sim 2.2 \times 10^{35}$ erg and were found to be closely associated with large stellar spots. One moderate amplitude flare was detected at a phase $\phi = 0.98$, probably emitting from the secondary component. Most of the flares were observed out of the eclipse phase which lead to the increasing complexity of constraining the stellar source among the binary companion. We noted that flare energy and stellar radius are in correlation as predicted by the theoretical equation ($E \propto R^3$). We calculated the flare energy due to the stellar spot and noticed that a magnetic field strength of $B \geq 500$ G is needed to trigger the observed superflares. Assuming the orbital period as the rotation period of binary components, we observed that this system exhibits low flaring activity which is also seen in few other systems and cannot be entirely attributed to the binary nature as this phenomenon is observed in single rapidly rotating stars. The estimated loop lengths for both stellar components, if interacting can probably explain superflares. Overall the present study indicates that superflares in DV Psc can be due to large stellar spot coverage over the stellar surface or interacting magnetic field between the components that can trigger them.

8 Acknowledgments

K.S. acknowledges the financial support from the SERB Core Research Grant project, the Government of India. Mamatha Rani acknowledges the support from the SRF INSPIRE (IF 170314) fellowship program, Government of India. The authors acknowledge also the TESS consortium for providing excellent observational data. Funding for the TESS mission is provided by NASAs Science Mission directorate. The data is publicly available from the Mikulski Archive for Space Telescopes.

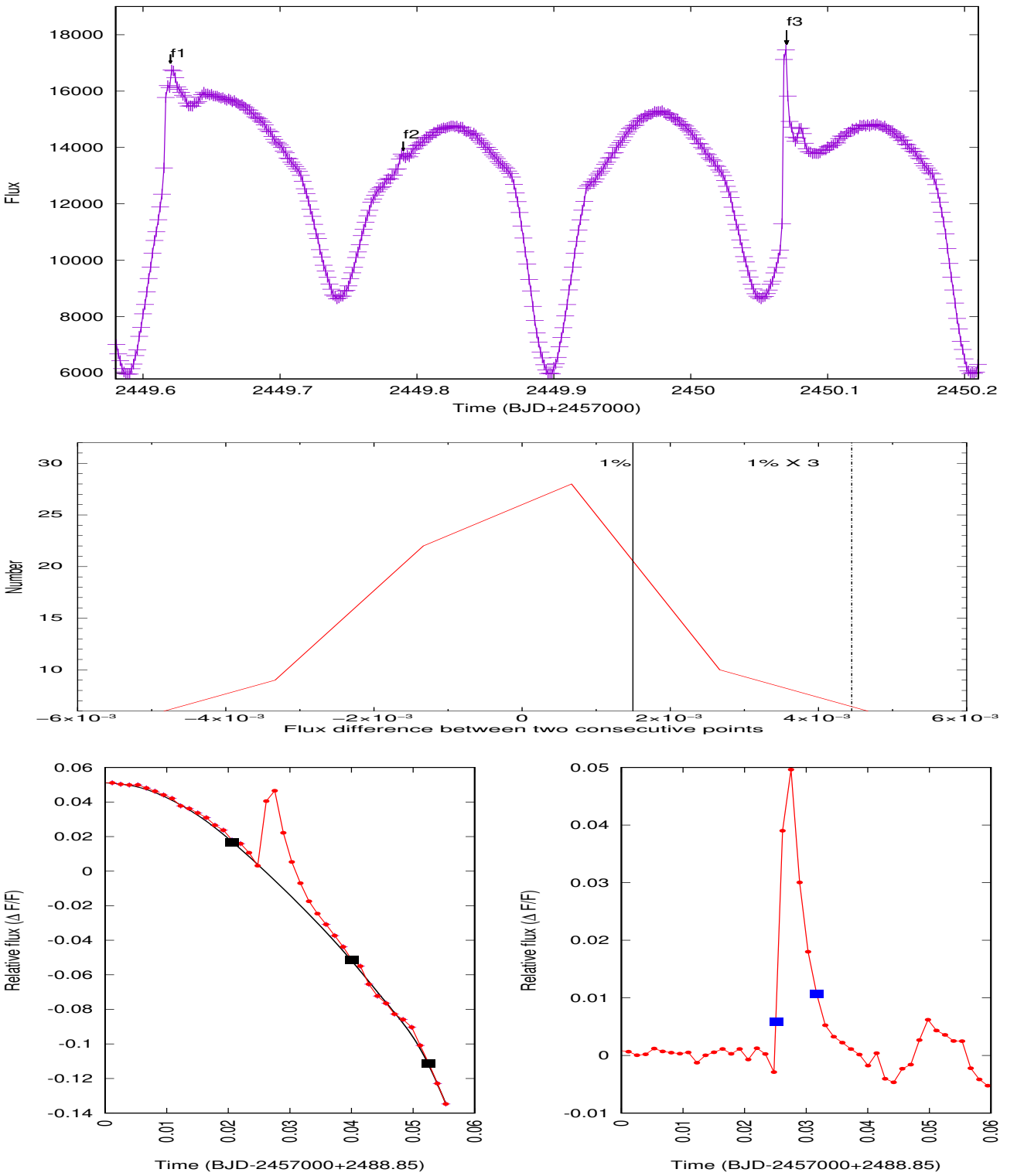

Fig. 1 : Top Panel: A section of DV Psc light curve observed from TESS along with two super flares f1 and f3 and a moderate flare f2. The histogram obtained by the flux difference between the consecutive points of the brightness variation is shown in the middle panel. The threshold for flare detection was set to 3 times the 1% (dot dashed line) and 1% represents the top of the flare (thick line) . The bottom left panel is the spline fit (thick line) to remove the average brightness where three black points are five average points before and after the flare f1 (see text for details). , the detection of flare f1 is shown in the bottom right panel after removing the average brightness and blue squares display the start and end times.

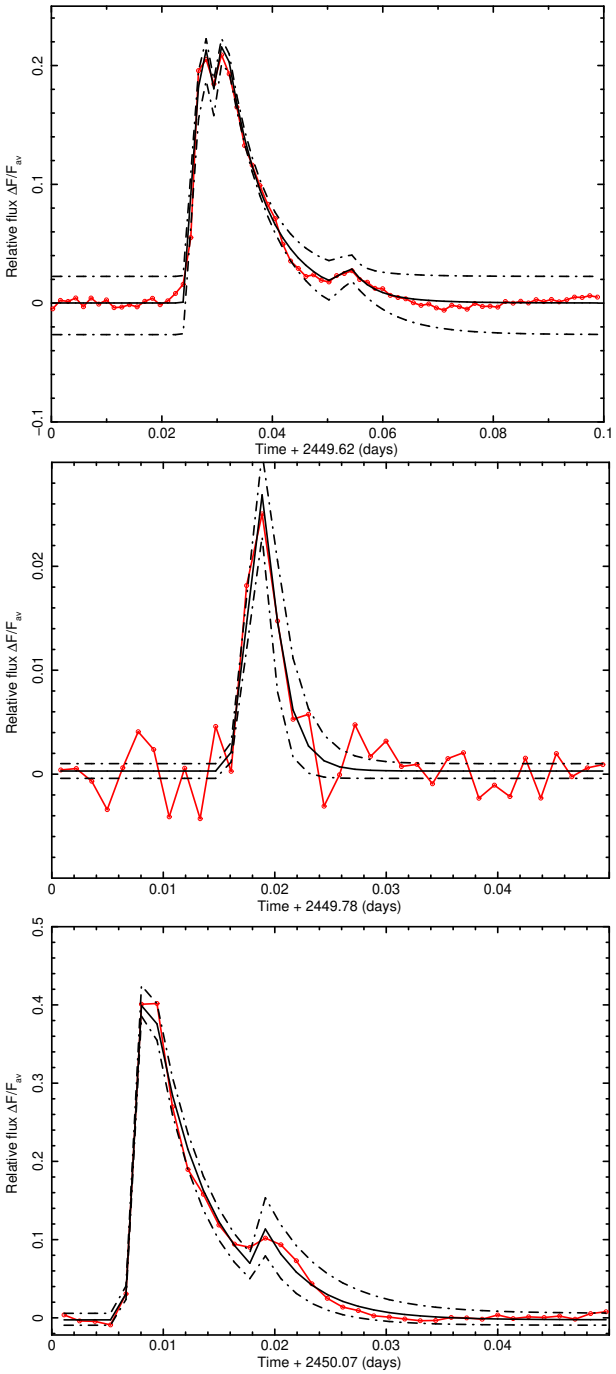

Fig. 2 : Fitted flares emitted by DV PSc f1, f2, and f3 (top to bottom). The thick line is the best fit of the FRED profile along with dashed lines showing the 90% Confidence interval.

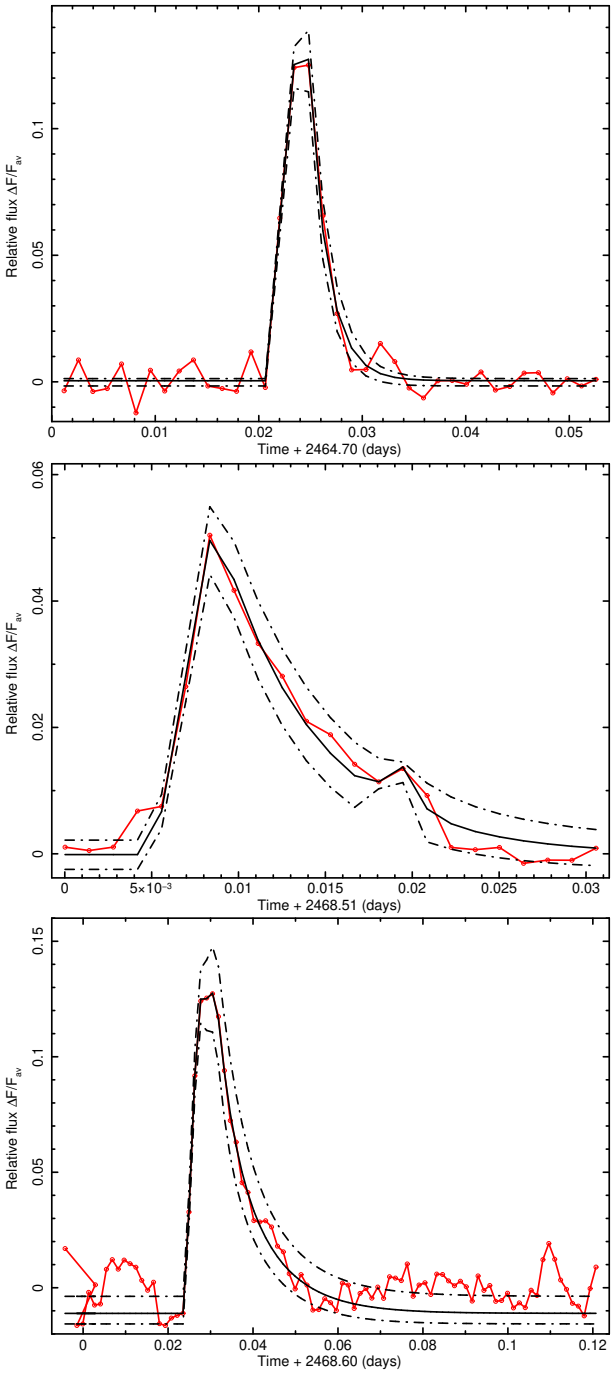

Fig. 3 : Top to bottom panels show the flares f4, f5 and f6 along with their best fits.

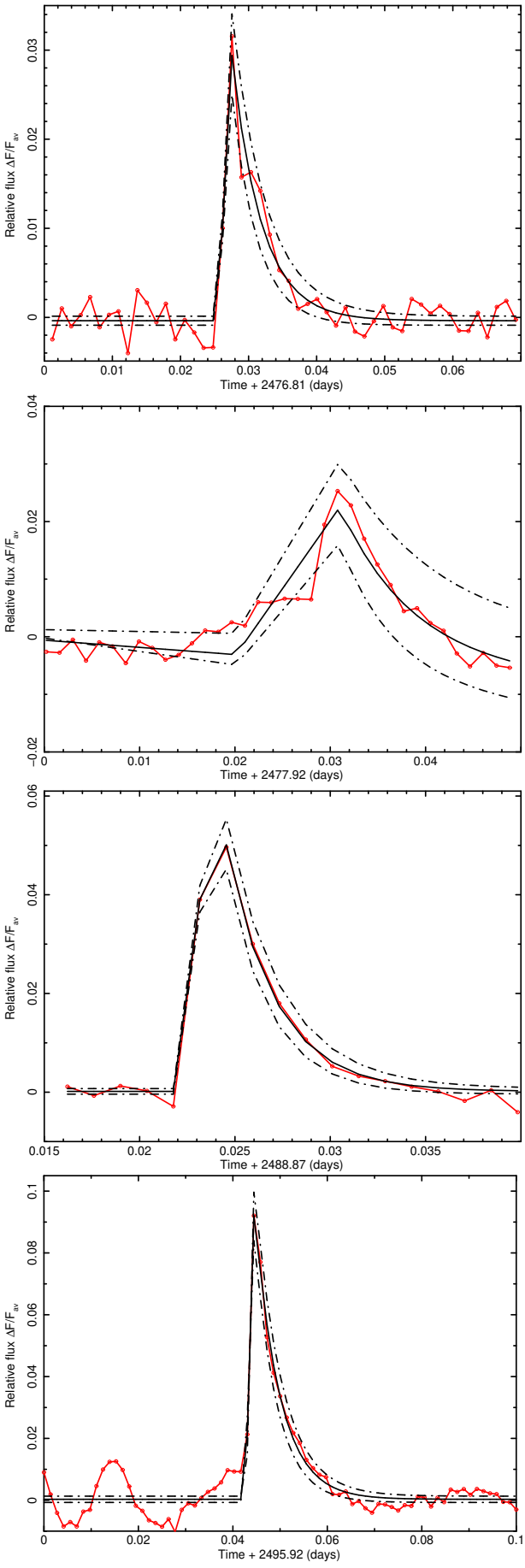

Fig. 4 : Same as above figure for f7, f8, f9 and f10 (top to bottom panels).

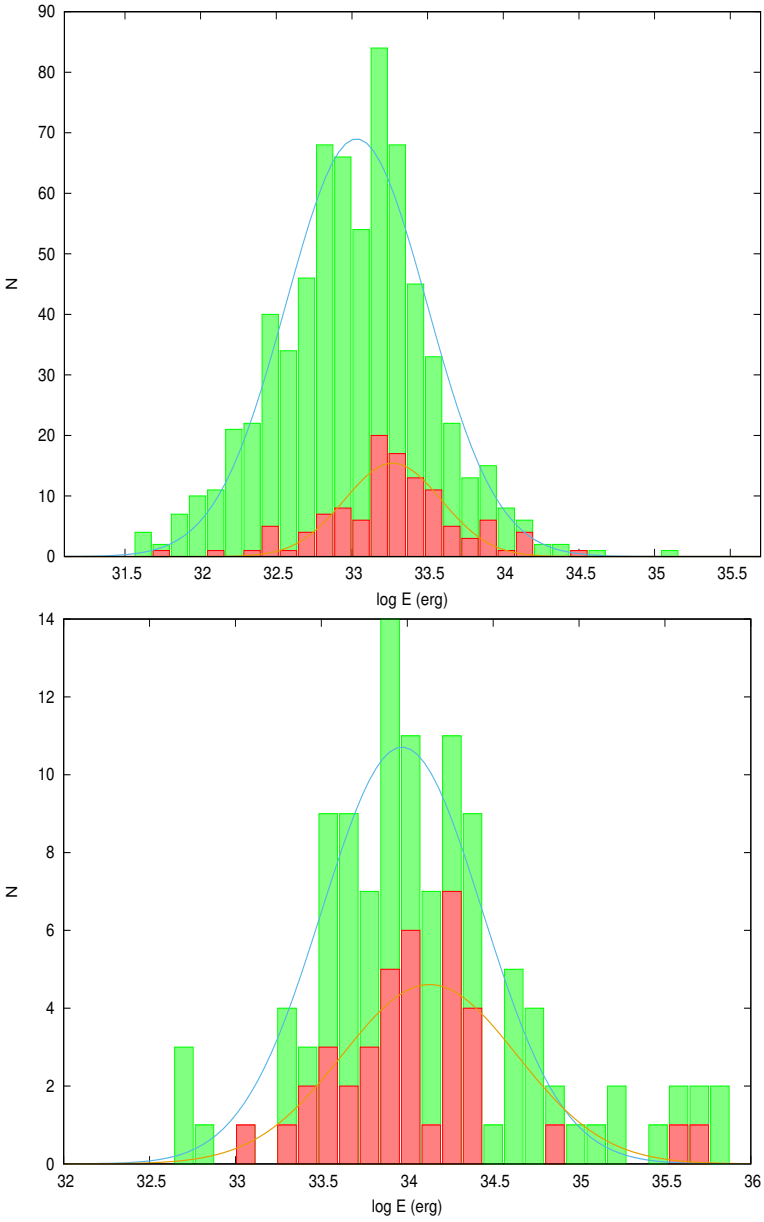

Fig. 5 : the top panel shows the histogram for M-type stars for a temperature bin of 3000-4000K (green) and 3350-3850 K and the bottom panel displays the histogram for K-type stars for a temperature bin of 4000-5000 K (green) and 4450-4850 K (red). The thick lines are the best Gaussian fits (for more details see section 6.3).

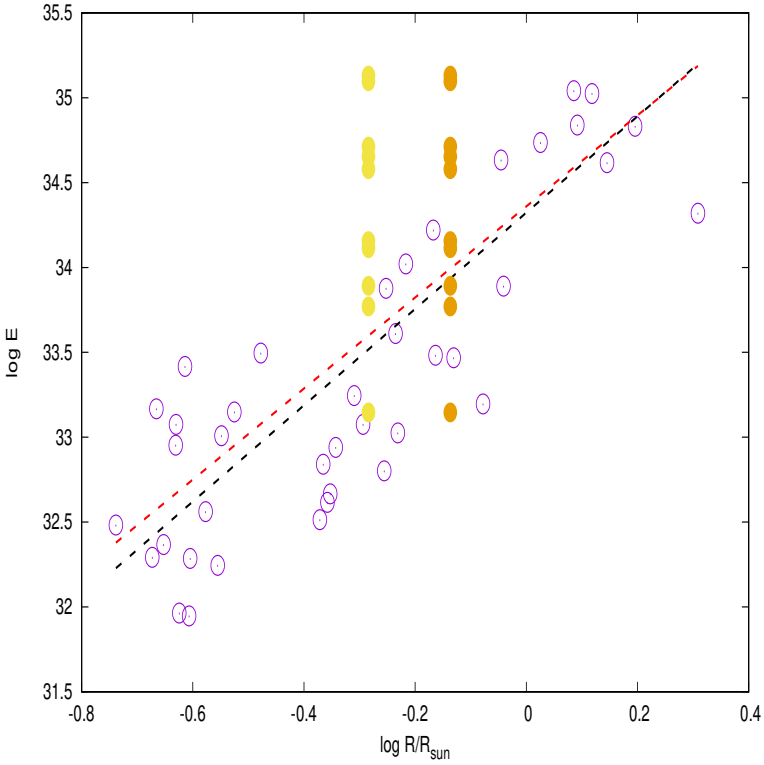

Fig. 6 : Radius–Energy plot, blue open circle data taken from Gunther et al. (2020), yellow for primary radius, orange for secondary radius (filled circles). The blue line is best the fit linear fit with a slope of 2.8 and the green line corresponds to a slope of 2.6 (see text for more details).

Table 1 : TESS flare parameters for the source DV Psc. Here, st and et are the start and end times based on Shibayama's method. st_f, pt_f, and τ_{decay} are start, peak, and decay times, based on FRED profile fits (see text). ϕ is a phase of the binary where the respective flare occurred. The time has the units of days. χ^2_{red} is reduced χ^2 for the best-fit of flare.

Flares	Time(BJD-2457000)	st	et	$\Delta F/F_{av}$	st_f	pt_f	τ_{decay}	ϕ	χ^2_{red}
		SHIBAYAMA's Method			BURST profile fit				
f1	2449.62	0.023	0.064	0.2000	0.025±0.0002	0.027±0.0001	0.01001±0.0003	0.10	0.99
f2	2449.78	0.014	0.037	0.0224	0.016±0.0005	0.019±0.0003	0.0016±0.0006	0.64	0.96
f3	2450.07	0.006	0.029	0.3748	0.007±0.0001	0.008±0.0001	0.0074±0.0003	0.55	1.10
f4	2464.70	0.021	0.030	0.144	0.021±0.0003	0.024±0.0002	0.0018±0.0003	0.98	0.96
f5	2468.51	0.218	0.581	0.0410	0.005±0.0003	0.009±0.0002	0.0055±0.0005	0.32	0.93
f6	2468.60	0.024	0.049	0.118	0.024±0.0005	0.029±0.0004	0.0086±0.0008	0.64	0.99
f7	2476.81	0.025	0.039	0.0065	0.026±0.0001	0.027±0.0002	0.0043±0.0004	0.24	0.98
f8	2477.92	0.016	0.054	0.0244	0.019±0.0002	0.033±0.0008	0.0038±0.0010	0.81	1.13
f9	2488.87	0.025	0.031	0.0458	0.022±0.0003	0.024±0.0002	0.0026±0.0003	0.32	1.12
f10	2495.92	0.033	0.062	0.0873	0.043±0.0002	0.044±0.0004	0.0052±0.0005	0.17	0.98

Table 2 : Flare parameters for DV Psc with primary component. The area of flare ($A_{\rm f}$) in the units of 10^{19} cm^2. Flare luminosity ($L_{\rm f}$) is in the units of 10^{31}erg s^{-1}. Energy of the flare i.e. $E_{\rm f}$, in the units of 10^{34} erg.

parameters	f1	f2	f3	f4	f5	f6	f7	f8	f9	f10
A_f	11.06	1.23	20.91	7.96	2.27	6.52	0.36	1.34	2.53	4.82
L_f	6.27	0.70	11.85	4.51	1.29	3.70	0.20	0.76	1.43	2.73
$E_f(=\int L_f(t)\ dt)$	22.22	1.39	23.97	4.29	2.31	8.02	0.24	2.55	1.05	6.67

Table 3 : Flare parameters for DV Psc with the secondary component. The area of flare ($A_{\rm f}$) in the units of 10^{19} cm^2. Flare luminosity ($L_{\rm f}$) is in the units of 10^{31}erg s^{-1}. Energy of the flare i.e. $E_{\rm f}$, in the units of 10^{34} erg.

parameters	f1	f2	f3	f4	f5	f6	f7	f8	f9	f10
A_f	6.22	0.69	11.76	3.36	1.27	3.67	0.20	0.75	1.42	2.71
L_f	3.52	0.39	6.66	1.91	0.72	2.08	0.11	0.43	0.80	1.54
$E_f(=\int L_f(t)\ dt)$	12.50	0.78	13.48	5.15	1.30	4.51	0.14	1.43	0.59	3.80

Bade, N., Engels, D., Voges, W., et al. 1998, AAS, 127, 145
Balona, L. A. 2015, Mon. Not. R. Astron. Soc., 447, 2714. doi:10.1093/mnras/stu2651
Beers, T. C., Bestman, W., Wilhelm, R. 1994, AJ, 108, 268
Berdyugina, S. V. 2005, LRSP, 2, 8
Cuntz, M., Saar, S. H., & Musielak, Z. E. 2000, ApJL, 533, L151
Davenport, J. R. A., Covey, K. R., Clarke, R. W., et al. 2019, ApJ, 871, 241
Dempsey, R. C., Linsky, J. L., Fleming, T. A.,& Schmitt, J. H. M. M. 1993, ApJS, 86, 599
Dimitrov, D. P., & Kjurkchieva, P. D. 2010, MNRAS, 406, 2559
Donati, J. F. 1999, MNRAS, 302, 457
Doyle L., Ramsay G., Doyle J. G., Wu K. and Scullion E. 2018 MNRAS 480 2153
Doyle, L., Ramsay, G., Doyle, J. G., & Wu, K., 2019, MNRAS, 435
Doyle L., Ramsay G., Doyle J. G., J Gerry Doyle, J. G., & Hakala, P., 2022 MNRAS 512, 979
Drake, S. A., Simon, T., & Linsky, J. L. 1989, ApJS, 71, 905
Gazeas, K. & Palafouta, S. 2019, Acta Astron., 69, 261.
Gao, Q., Xin, Y., Liu, J. F., Zhang, X. B., and Gao, S., 2016, ApJS, 224, 37
Gunther, M., Zhan, Z., Seager, S., et al. 2020, AJ, 159, 60
Hawley S. L., and Pettersen B. R., 1991, ApJ, 378, 725
Hawley, S. L., Davenport, J. R. A., Kowalski, A. F., et al., 2014, ApJ, 797, 121
He, H., Wang, H., Zhang, M., et al. 2018, ApJS, 236, 7
Herbst, K., Papaioannou, A., Airapetian, V. S., Atri, D. M. 2021, ApJ 907, 89
Hilton, E. J., Hawley, S. L., & Kowalski, A. F. 2011,
Honda, S., Notsu, Y., Namekata, K., et al. 2018, ApSS, 70, 62
Holzwarth, V., & Schüssler, M. 2003a, A&A, 405, 291
Holzwarth, V., & Schüssler, M. 2003b, A&A, 405, 303
Howard, W. S., Tilley, M. A., Corbett, H., et al. 2018, ApJL, 860, L30
Howard, W. S., Corbett, H., Law, N. M., et al. 2020, ApJ, 895, 140
Ip, W.-H., Kopp, A., & Hu, J.-H. 2004, ApJL, 602, L53
Kiraga M., Stepien K., 2007, Acta Astron., 57, 149
Kochukhov, O., Mantere, M. J., Hackman, T. and Ilyin, I. 2013, A&A, 550, 84
Kowalski, A. F., Hawley, S. L., Holtzman, J. A., Wisniewski, J. P., & Hilton, E. J. 2010, ApJL, 714, L98
Kowalski, A. F., Hawley, S. L., Wisniewski, J. P., et al. 2013, ApJS, 207, 15
Kuznetsov, A. A., & Kolotkov, D. Y. 2021, ApJ, 912, 81
Lin, C. L., Ip, W. H., Hou, W. C., Huang, L., C., & Chang, H. Y. 2019, ApJ, 873, 97
Lu, W. X., Rucinski, S. M., Ogloza, W. 2001, AJ, 122, 402
Maehara, H., Shibayama, T., Notsu, S., et al. 2012, Nature, 485, 478
Maehara, H., Notsu, Y., Notsu, S., et al. 2017, PASJ, 69, 41

Maggio A., Sciortino S., Vaiana G. S., Majer P., Bookbinder J., Golub L., Harnden F. R. Jr, Rosner R., 1987, ApJ, 315, 687
Namekata, K., et al. 2022, Nature Astronomy, 6, 241
Notsu, Y., Maehara, H., Honda, S., et al. 2019, ApJ, 876, 58
Noyes, R. W., Hartmann, L. W., Baliunas, S. L., et al. 1984, Astrophys. J., 279, 763. doi:10.1086/161945
Pandey, J.C.,& Singh, K. P., 2012, MNRAS, 419, 1219
Parimucha, Š., Pribulla, T., Rucinski, S., et al. 2010, in ASP Conf. Ser. 435,
Petit, P., Donati, J., Wade, G. A., et al. 2004, MNRAS, 348, 1175
Pi, Q. F., Zhang, L. Y., Li, Z. M., et al. 2014, AJ, 147, 50
Pi, Q., feng ., Zhang, L., yun ., Bi, S., lan ., et al. 2019, Astrophys. J., 877, 75.
Qian, S. B., Zhang, J., & Zhu, L. Y. 2012, MNRAS, 423, 3646
Ricker, G. R., Winn, J.N., Vanderspek, R., et al. 2015, Journal of Astronomical Telescopes, Instruments, and Systems, 1, 014003
Robb, R. M., Wagg, J., Berndsen, A., et al. 1999, IBVS, 4800, 1
Rubenstein, E. P., & Schaefer, B. E. 2000, ApJ, 529, 1031
Salchi, F., Edalati, M. T. 2003, ApSS, 288, 217
Shibata, K. & Magara, T. 2011, Living Reviews in Solar Physics, 8, 6. doi:10.12942/lrsp-2011-6
Shibata, K., Isobe, H., Hillier, A., et al. 2013, PASJ, 65, 49
Shibayama, T., Maehara, H., Notsu, S., et al. 2013, Astrophys. J. Suppl. Ser., 209, 5. doi:10.1088/0067-0049/209/1/5
Shulyak, D., et al. 2019, A&A, 626, A28
Simon T., Linsky J. L. and Schiffer F. H. III 1980 ApJ 239 911
Smelcer, L., Wolf, M., Kucakova, H., et al. 2017, MNRAS, 466, 2542
Sriram, K., Vijaya, A., Lahiri, D., et al. 2023, Publ. Astron. Soc. Jpn., 75, 476. doi:10.1093/pasj/psad013
Stephenson, C. B. 1986, AJ, 92, 139

Torres, G, Fieden, G. A., Vanderburg, A., and Curtis, J. L., 2022, Galaxies, 10(1), 3
Vaňko, M., Parimucha, Š., Pribulla, T. 2007, AN, 328, 655
Wright, N. J., Newton, E. R., Williams, P. K. G., Drake, J. J., & Yadav, R. K. 2018, MNRAS, 479, 2351
Yang, H. Q., Liu, J. F., Gao, Q., et al. 2017, ApJ, 849, 36
Zhang, X. B., Zhang, R. X. 2007, MNRAS, 382, 1133

References

Abolmasov, P., Poutanen, J.: Astronomy and Astrophysics **647**, 45 (2021)

Abolmasov, P., Nättilä, J., Poutanen, J.: Astronomy and Astrophysics **638**, 142 (2020)

Agrawal, P., Yadav, J., Antia, H., Dedhia, D., Shah, P., Chauhan, J.V., Manchanda, R., Chitnis, V., Gujar, V., Katoch, T., *et al.*: Journal of Astrophysics and Astronomy **38**(2), 1 (2017)

Agrawal, V., Misra, R.: Monthly Notices of the Royal Astronomical Society **398**(3), 1352 (2009)

Antia, H., Yadav, J., Agrawal, P., Chauhan, J.V., Manchanda, R., Chitnis, V., Paul, B., Dedhia, D., Shah, P., Gujar, V., *et al.*: The Astrophysical Journal Supplement Series **231**(1), 10 (2017)

Babkovskaia, N., Brandenburg, A., Poutanen, J.: Monthly Notices of the Royal Astronomical Society **386**(2), 1038 (2008)

Bhattacharyya, S., Yadav, J.S., Sridhar, N., Verdhan Chauhan, J., Agrawal, P.C., Antia, H.M., Pahari, M., Misra, R., Katoch, T., Manchanda, R.K., Paul, B.: The Astrophysical Journal **860**(2), 88 (2018)

Chiranjeevi, P., Sriram, K.: Monthly Notices of the Royal Astronomical Society **516**(2), 2500 (2022)

Dauser, T., García, J., Walton, D.J., Eikmann, W., Kallman, T., McClintock, J., Wilms, J.: Astronomy and Astrophysics **590**, 76 (2016)

Di Salvo, T., Iaria, R., Burderi, L., Robba, N.R.: The Astrophysical Journal **542**(2), 1034 (2000)

Egron, E., di Salvo, T., Burderi, L., Papitto, A., Barragán, L., Dauser, T., Wilms, J., D'Aì, A., Riggio, A., Iaria, R., Robba, N.R.: Astronomy and Astrophysics **530**, 99 (2011)

García, J., Dauser, T., Lohfink, A., Kallman, T.R., Steiner, J.F., McClintock, J.E., Brenneman, L., Wilms, J., Eikmann, W., Reynolds, C.S., Tombesi, F.: The Astrophysical Journal **782**(2), 76 (2014)

Gilfanov, M., Revnivtsev, M., Molkov, S.: Astronomy and Astrophysics **410**(1), 217 (2003)

Hasinger, G., van der Klis, M.: Astronomy and Astrophysics **225**, 79 (1989)

Kubota, A., Makishima, K., Ebisawa, K.: The Astrophysical Journal **560**(2), 147 (2001)

Kubota, A., Tanaka, Y., Makishima, K., Ueda, Y., Dotani, T., Inoue, H., Yamaoka, K.: Publications of the Astronomical Society of Japan **50**(6), 667 (1998)

Lei, Y.J., Qu, J.L., Song, L.M., Zhang, C.M., Zhang, S., Zhang, F., Wang, J.M., Li, Z.B., Zhang, G.B.: The Astrophysical Journal **677**(1), 461 (2008)

Lei, Y.-J., Zhang, H.-T., Zhang, C.-M., Qu, J.-L., Yuan, H.-L., Dong, Y.-Q., Zhao, Y.-H., Wang, D.-H., Yin, H.-X., Zhang, Y.-X., Song, L.-M.: The Astronomical Journal **146**(3), 60 (2013)

Lei, Y.-J., Zhang, S., Qu, J.-L., Yuan, H.-L., Wang, Y.-N., Dong, Y.-Q., Zhang, H.-T., Li, Z.-B., Zhang, C.-M., Zhao, Y.-H.: The Astronomical Journal **147**(3), 67 (2014)

Malu, S., Sriram, K., Agrawal, V.: Monthly Notices of the Royal Astronomical Society **499**(2), 2214 (2020)

Malu, S., Sriram, K., Harikrishna, S., Agrawal, V.K.: Monthly Notices of the Royal Astronomical Society **506**(4), 6203 (2021a)

Malu, S., Harikrishna, S., Sriram, K., Agrawal, V.K.: Astrophysics and Space Science **366**(9), 1 (2021b)

Manmoto, T., Mineshige, S., Kusunose, M.: The Astrophysical Journal **489**(2), 791 (1997)

Maoz, D., Netzer, H.: Monthly Notices of the Royal Astronomical Society **236**(1), 21 (1989)

McKinney, J.C., Tchekhovskoy, A., Blandford, R.D.: Monthly Notices of the Royal Astronomical Society **423**(4), 3083 (2012)

Mondal, A.S., Pahari, M., Dewangan, G.C., Misra, R., Raychaudhuri, B.: Monthly Notices of the Royal Astronomical Society **466**(4), 4991 (2017)

Ng, C., Trigo, M.D., Bel, M.C., Migliari, S.: Astronomy and Astrophysics **522** (2010)

Pen, U.-L., Matzner, C.D., Wong, S.: The Astrophysical Journal **596**(2), 207 (2003)

Piraino, S., Santangelo, A., Kaaret, P.: Astronomy and Astrophysics **360**, 35 (2000)

Popham, R., Sunyaev, R.: The Astrophysical Journal **547**(1), 355 (2001)

Psaltis, D., Belloni, T., van der Klis, M.: The Astrophysical Journal **520**(1), 262 (1999)

Revnivtsev, M.G., Gilfanov, M.R.: Astronomy and Astrophysics **453**(1), 253 (2006)

Seifina, E., Titarchuk, L.: The Astrophysical Journal **738**(2), 128 (2011)

Shakura, N.I., Sunyaev, R.A.: Astronomy and Astrophysics **24**, 337 (1973)

Shaposhnikov, N., Titarchuk, L., Haberl, F.: Astrophysical Journal Letters **593**(1), 35 (2003)

Shimura, T., Takahara, F.: The Astrophysical Journal **445**, 780 (1995)

Sleator, C.C., Tomsick, J.A., King, A.L., Miller, J.M., Boggs, S.E., Bachetti, M., Barret, D., Chenevez, J., Christensen, F.E., Craig, W.W., Hailey, C.J., Harrison, F.A., Rahoui, F., Stern, D.K., Walton, D.J., Zhang, W.W.: The Astrophysical Journal **827**(2), 134 (2016)

Sriram, K., Choi, C., Rao, A.: The Astrophysical Journal Supplement Series **200**(2), 16 (2012)

Sriram, K., Malu, S., Choi, C.: The Astrophysical Journal Supplement Series **244**(1), 5 (2019)

Sriram, K., Agrawal, V., Pendharkar, J.K., Rao, A.: The Astrophysical Journal **661**(2), 1055 (2007)

Sriram, K., Chiranjeevi, P., Malu, S., Agrawal, V.: Journal of Astrophysics and Astronomy **42**(2), 1 (2021)

Tarana, A., Belloni, T., Bazzano, A., Méndez, M., Ubertini, P.: Monthly Notices of the Royal Astronomical Society **416**(2), 873 (2011)

van der Klis, M.: In: X-ray Binaries, p. 252 (1995)

van der Klis, M.: In: Strohmayer, T.E. (ed.) Rossi2000: Astrophysics with the Rossi X-ray Timing Explorer 2000

van der Klis, M.: A review of rapid X-ray variability in X-ray binaries. arXiv (2004)

Verdhan Chauhan, J., Yadav, J.S., Misra, R., Agrawal, P.C., Antia, H.M., Pahari, M., Sridhar, N., Dedhia, D., Katoch, T., Madhwani, P., Manchanda, R.K., Paul, B., Shah, P.: The Astrophysical Journal **841**(1), 41 (2017)

Wang, Y., Méndez, M., Sanna, A., Altamirano, D., Belloni, T.M.: Monthly Notices of the Royal Astronomical Society **468**(2), 2256 (2017)

Wang, Y., Méndez, M., Altamirano, D., Zhang, G., Belloni, T.M., Ribeiro, E.M., Linares, M., Sanna, A., Motta, S.E., Tomsick, J.A.: Monthly Notices of the Royal Astronomical Society **484**(3), 3004 (2019)

Wang, De-Hua, Zhang, Cheng-Min, Qu, Jin-Lu: A&A **618**, 181 (2018)

Wijnands, R., van der Klis, M.: The Astrophysical Journal **514**(2), 939 (1999)

Yadav, J., Agrawal, P., Antia, H., Chauhan, J.V., Dedhia, D., Katoch, T., Madhwani, P., Manchanda, R., Misra, R., Pahari, M., *et al.*: In: Space Telescopes and Instrumentation 2016: Ultraviolet to Gamma Ray, vol. 9905, p. 374 (2016). SPIE